Diameter-Controlled and Nitrogen-Doped Vertically Aligned Single-Walled Carbon Nanotubes

Theerapol Thurakitseree[a], Christian Kramberger[a], Pei Zhao[a], Shinya Aikawa[a], S. Harish[a], Shohei Chiashi[a], Erik Einarsson[a,b], Shigeo Maruyama[a*]

[a]*Department of Mechanical Engineering, The University of Tokyo, 7-3-1 Hongo, Bunkyo-ku, Tokyo 113-8656, Japan*

[b]*Global Center of Excellence for Mechanical Systems Innovation, The University of Tokyo, 7-3-1 Hongo, Bunkyo-ku, Tokyo 113-8656, Japan*

Abstract

Diameter controlled and vertically aligned single-walled carbon nanotubes were synthesized from pure and mixed ethanol/acetonitrile feedstock. With increasing acetonitrile concentration in the feedstock, nitrogen incorporation into the sp^2 carbon network increased until saturating at approximately one atomic percent. The incorporation of nitrogen correlates with a significant diameter reduction from a mean diameter of 2.1 nm down to 0.7 nm. Heteroatom-mediated diameter control is independent of catalyst preparation and represents a versatile tool for the direct synthesis of tailored single-walled carbon nanotubes.

[*] Corresponding author: Tel. +81-3-5841-6421; fax: +81-3-5800-6983. *E-mail Address: maruyama@photon.t.u-tokyo.ac.jp* (S. Maruyama).

1. Introduction

The ability to tune the electrical and optical properties of single-walled carbon nanotubes (SWCNT) is a long-standing goal of SWCNT synthesis. SWCNT synthesized by conventional methods are inherently devoid of chirality control. However, their electronic properties may be controlled indirectly by narrowing the diameter range to confine the range of possible chiralities. Supporting materials and templates [1-6] have been used to influence the diameter of SWCNT via catalyst morphology or cap formation [7], although these nanotubes still require additional post-processing in order to extract them from the supporting (powder) materials. A potentially non-templated approach to control the SWCNT diameter is by the choice of carbon feedstock, such as carbon monoxide [1, 3], ethanol [2], methane [8], acetylene [9], ethylene [10], or other organic chemical sources [11]. Acetonitrile (CH_3CN) has been used to synthesize nitrogen (N)-doped carbon nanotubes [12-20], and some groups have reported a reduction in SWCNT diameter due to the presence of nitrogen [13, 15]. Pint and co-workers [16] have also recently scaled up N-doped SWCNT synthesis by a water-assisted approach using acetonitrile as the C/N feedstock.

Here we employ pure and mixed ethanol and/or acetonitrile feedstocks to grow vertically aligned SWCNT by no-flow chemical vapor deposition (CVD) from Co/Mo binary catalyst. The mean diameters of the vertically aligned SWCNT synthesized from identically prepared catalyst particles are as different as 2.1 nm for pure ethanol feedstock and 0.7 nm for pure acetonitrile feedstock. If a mixed feedstock is employed, the atomic nitrogen concentration saturates at 1.2 at.%. This saturation correlates with the decrease in mean diameter.

2. Experimental

Vertically aligned SWCNT arrays [21] were synthesized from Co/Mo binary catalyst by a no-flow CVD process [22] using mixtures of acetonitrile and ethanol as the carbon feedstock. This mixture was varied from 0 to 100% acetonitrile by volume (hereafter just %), and all other parameters were kept unchanged as reported in Ref. [22]. Catalyst was loaded onto fused quartz substrates by dip-coating into separate solutions of Mo-acetate and Co-acetate dissolved in ethanol (metal species content 0.01 wt.% each). The process is based on that described in Ref. [23]. During heating of the CVD system, the Co/Mo binary catalyst were reduced under Ar containing 3% H_2 at a flow rate of 300 sccm and a pressure of 40 kPa. After reaching the growth temperature of 800˚C in 25 min, the system was evacuated and then sealed before introducing 40 μL of feedstock. The feedstock was introduced all at once, but the vapor pressure soon stabilized at approximately 1.7 kPa. The reaction time was 3 min in all cases, and after synthesis the CVD chamber was evacuated and cooled to room temperature while flowing 300 sccm Ar. As-grown vertically aligned SWCNT arrays were characterized by scanning electron microcopy (SEM, 1 kV acceleration voltage, S-4800, Hitachi Co., Ltd.), UV-vis-NIR absorption spectroscopy (UV-3150, Shimadzu Co., Ltd.) and resonance Raman spectroscopy (Chromex 501is with Andor DV401-FI) using excitation wavelengths of 488 and 633 nm. For transmission electron microscopy (TEM, JEOL 2000EX operating at 120 kV), the SWCNT were dispersed in ethanol and the dispersion was dropped onto Cu microgrids. For X-ray photoelectron spectroscopy (XPS, PHI 5000 VersaProbe, 14.86 keV), vertically aligned SWCNT arrays were transferred [24] onto a Si wafer (50 nm oxide layer) and heated to 250˚C for 10 min to dehydrate the sample. For further UV-vis-NIR and photoluminescence excitation spectroscopy (PLE, HORIBA Jobin Yvon Fluorolog *i*HR320, equipped with a liquid-nitrogen-cooled GaAs detector), SWCNT synthesized on USY-

zeolite powder [25, 26] using mixed feedstocks were dispersed in 5 mL D_2O with 1 wt.% sodium deoxycholate (DOC) surfactant. The fluorescence emission wavelength range was recorded from 900 to 1400 nm, while the excitation wavelength was scanned from 500 to 850 nm in 5 nm steps. After bath sonication for 10 min and an additional 30 min of ultrasonication (Hielscher Ultrasonics GmbH UP400S with H3/Micro Tip 3 at a power flux level of 400 $W \cdot cm^{-2}$), the suspension was centrifuged for 15 min at 85,000 rpm (327,000*g*). Finally the supernatant was extracted. The supernatant was also used for further XPS measurements of a SWCNT film formed by vacuum filtration [27]. The dispersed SWCNT film thickness was examined to be more than 30 μm.

3. Results and Discussions

The SEM micrographs in Fig. 1a clearly demonstrate the viability of pure acetonitrile and its mixtures for the synthesis of vertically aligned SWCNT on flat substrates. TEM images in Fig. 1b show clean SWCNT are obtained from both pure ethanol (left) and pure acetonitrile (right). In fact, no catalyst particles were encountered during TEM observations. Visual inspection of TEM micrographs show significantly narrower SWCNT are synthesized from pure acetonitrile feedstock.

Optical absorption spectra of as-grown vertically aligned SWCNT arrays (Fig. 2) reveal the E_{11}^S and E_{22}^S transitions in ethanol-grown SWCNT as well as the E_{11}^S transitions in small-diameter SWCNT synthesized from acetonitrile. The mean diameter was determined using the following empirical relation described in Ref. [28] (Fig. 2)

$$E_{ii}(p,d_t) = \beta_p \cos 3\theta / d_t^2 + ap/d_t[1 + b\log cd_t / p], \quad (1)$$

where β_p is 0.05 and -0.07 for E_{11}^S (p = 1) and E_{22}^S (p = 2) respectively. d_t is tube diameter in nm with chiral angle θ (from 0 to 30°), while a = 1.049 eV·nm, b = 0.456 and c = 0.812 nm^{-1}, and a lifetime broadening Γ of 65 meV was used [29]. The positions and widths of the

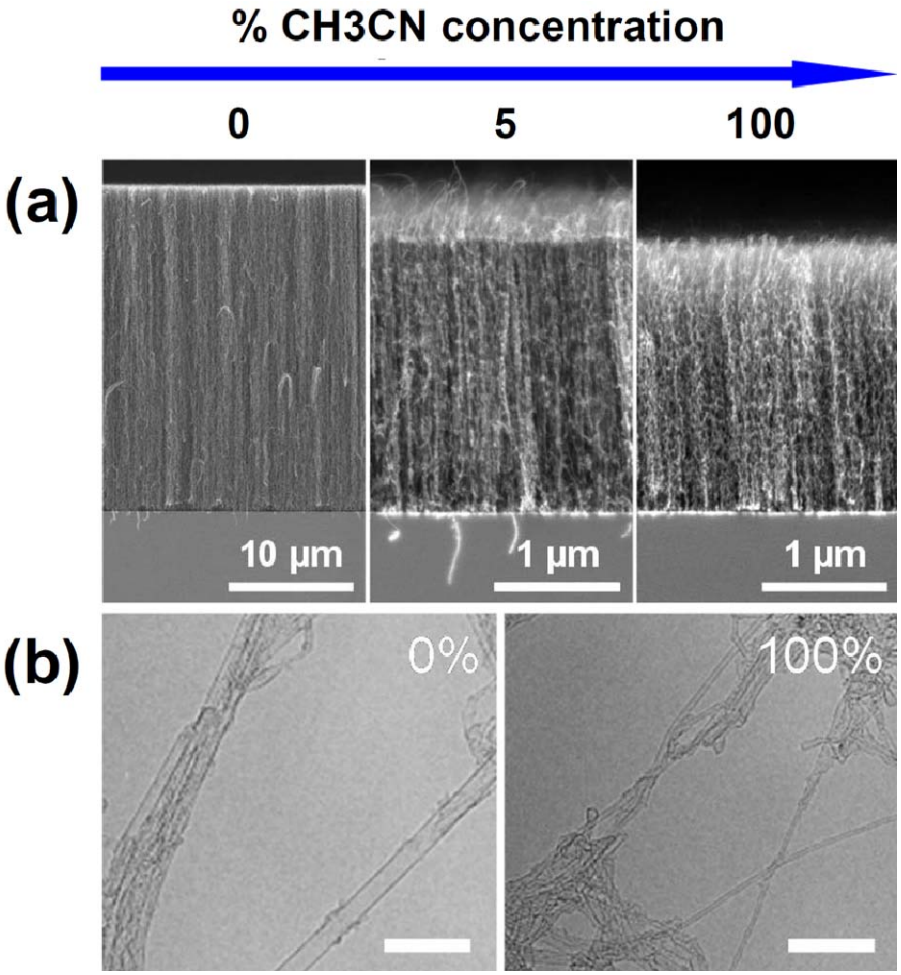

Fig. 1. (a) SEM micrographs of vertically aligned SWCNT arrays synthesized by no-flow CVD using different ethanol/acetonitrile mixed feedstocks (0, 5 and 100 vol.% acetonitrile). (b) TEM micrographs of SWCNT grown from pure acetonitrile (right panel) and pure ethanol (left panel). The vastly different diameters are directly visible (scale bar is 20 nm in both micrographs).

E_{11}^{S} and E_{22}^{S} peaks are reproduced by diameter distributions centered at 0.7 and 2.1 nm with full-width half-maxima (FWHM) of 0.24 and 0.6 nm for pure acetonitrile-grown and ethanol-grown SWCNT, respectively. The diameter of SWCNT synthesized from Co/Fe catalysts on zeolite powder [25, 26] using different mixed feedstock recipes was also found to be smaller than for pure ethanol.

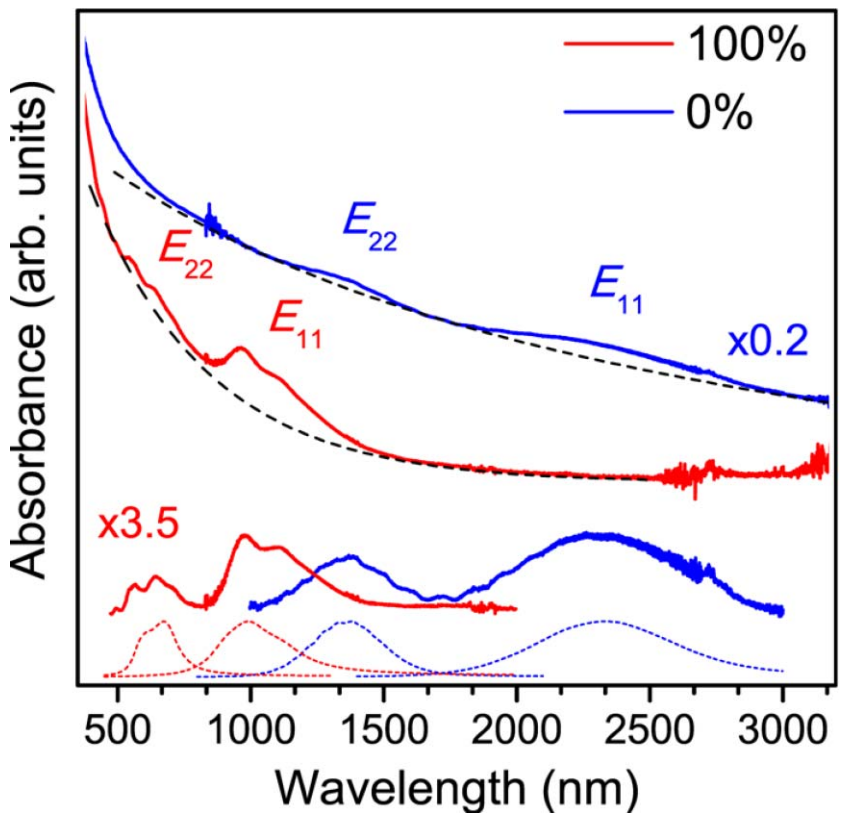

Fig. 2. UV-vis-NIR spectra of vertically aligned SWCNT grown from acetonitrile and ethanol. The black dashed lines represent exponential and hyperbolic background contributions for the case of acetonitrile and ethanol, respectively, and the lower spectra are after background subtraction. Mean diameters were determined from the empirical relation of electronic transition energy (red and blue dashed lines) to be 0.7 and 2.1 nm, respectively (see text).

A plot showing PLE peak area for different tube diameters is presented in Fig. 3. The PLE spectra were obtained from micelle-suspended SWCNT grown on zeolite support (see Supplementary data), and the normalized peak area was evaluated using the ratio of the area of each peak to the sum of the total peak areas ($A_{(n,m)} / \Sigma A_{(n,m)}$). Upon increasing the concentration of acetonitrile in the feedstock, the abundance of (6,5) and (7,5) nanotubes appears to increase, whereas the abundance decreases for (7,6) and (8,6) nanotubes. This is in

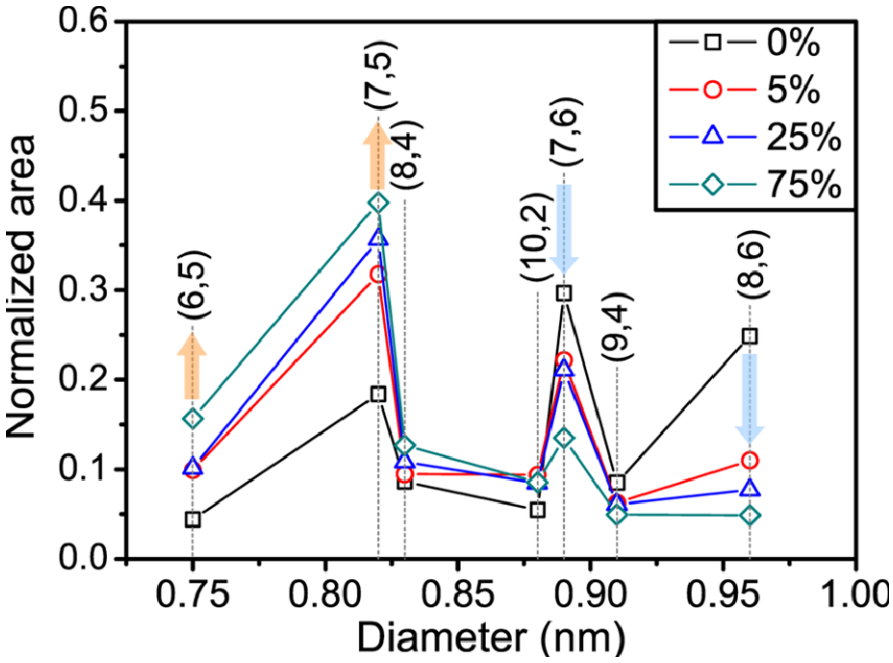

Fig. 3. Plot of normalized PLE peak areas versus tube diameter for dispersed SWCNT synthesized on zeolite powder using different feedstock mixtures (0 to 75 vol.% acetonitrile). The orange and blue arrows represent increasing and decreasing abundance with increasing concentration of acetonitrile feedstock.

agreement with the absorbance spectra indicating acetonitrile promotes the growth of small-diameter nanotubes.

Figure 4 shows the RBM, D and G lines in resonant Raman spectra measured using 633 nm laser excitation for different feedstock mixtures. The RBM frequency scales as the inverse of nanotube diameter according to $\omega_{RBM} \approx 217.8/d + 15.7$ [28]. The D line is only Raman active in the presence of lattice distortions. The splitting of the G line into G^+ and G^- peaks is diameter dependent [30], and the G^- is softened in small-diameter SWCNT [31, 32]. In these spectra, the large-diameter RBM peaks at ~190 cm^{-1} are predominant for marginal amounts of acetonitrile in the feedstock. However, this peak begins to diminish and a new RBM peak at ~280 cm^{-1} arises when the concentration of acetonitrile in the feedstock reaches

1%. After their sudden appearance, the small diameter RBM peaks at ~280 cm^{-1} grow gradually with increased acetonitrile concentrations in the feedstock.

According to the Kataura plot [28, 33], the excitation wavelength of 633 nm is in resonance with the E_{33}^{S} and E_{44}^{S} transitions [28] in large-diameter SWCNT, and the first metallic transition E_{11}^{M} gives rise to a subtle Fano resonance with a characteristic Breit-Wigner-Fano (BWF) lineshape. Upon adding more than 2% acetonitrile, the RBM peaks at ~190 cm^{-1} and the attributed Fano resonance vanish in concomitance. The frequency offset between the G^{+} and G^{-} lines is also increased. The changes in the G line for 488 nm excitation wavelength are complementary. Here the smaller diameters exhibit a strong Fano

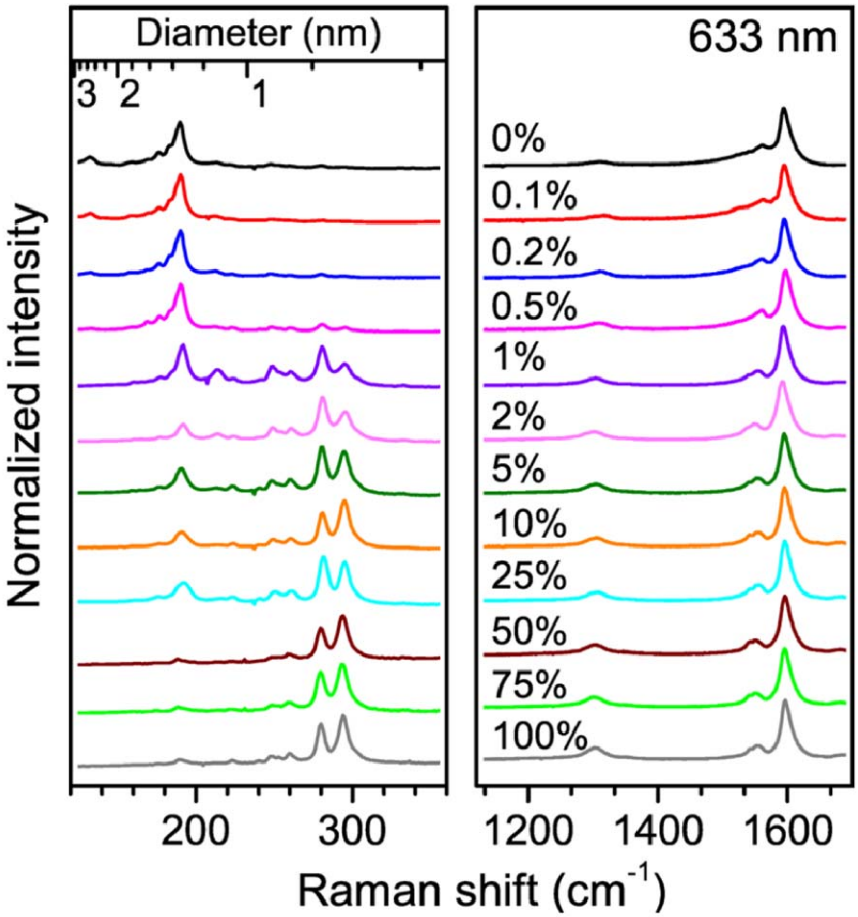

Fig. 4. Resonance Raman spectra at 633 nm excitation of vertically aligned SWCNT arrays grown using different acetonitrile concentrations. The tube diameter is evaluated from RBM peak positions using the relation $\omega_{RBM} \approx 217.8/d + 15.7$ [28].

resonance and the larger diameters are purely in semiconducting resonance (see Fig. 5a). It can be clearly seen that the Fano resonance emerges with increasingly small doses of acetonitrile. The position of the G^+ line is 1594 cm^{-1} for all samples and for both excitation wavelengths. The RBM peak positions confirm selective resonances with diameters between 0.7 and 1.0 nm when adequate amounts of acetonitrile are added to the feedstock, and diameters between 1.2 and 2.3 nm for pure ethanol.

For 633 nm excitation, the G/D ratios in the pure acetonitrile-grown and pure ethanol-grown SWCNT are 4.3 and 16.7, respectively. The ratios for mixed feedstocks fall between

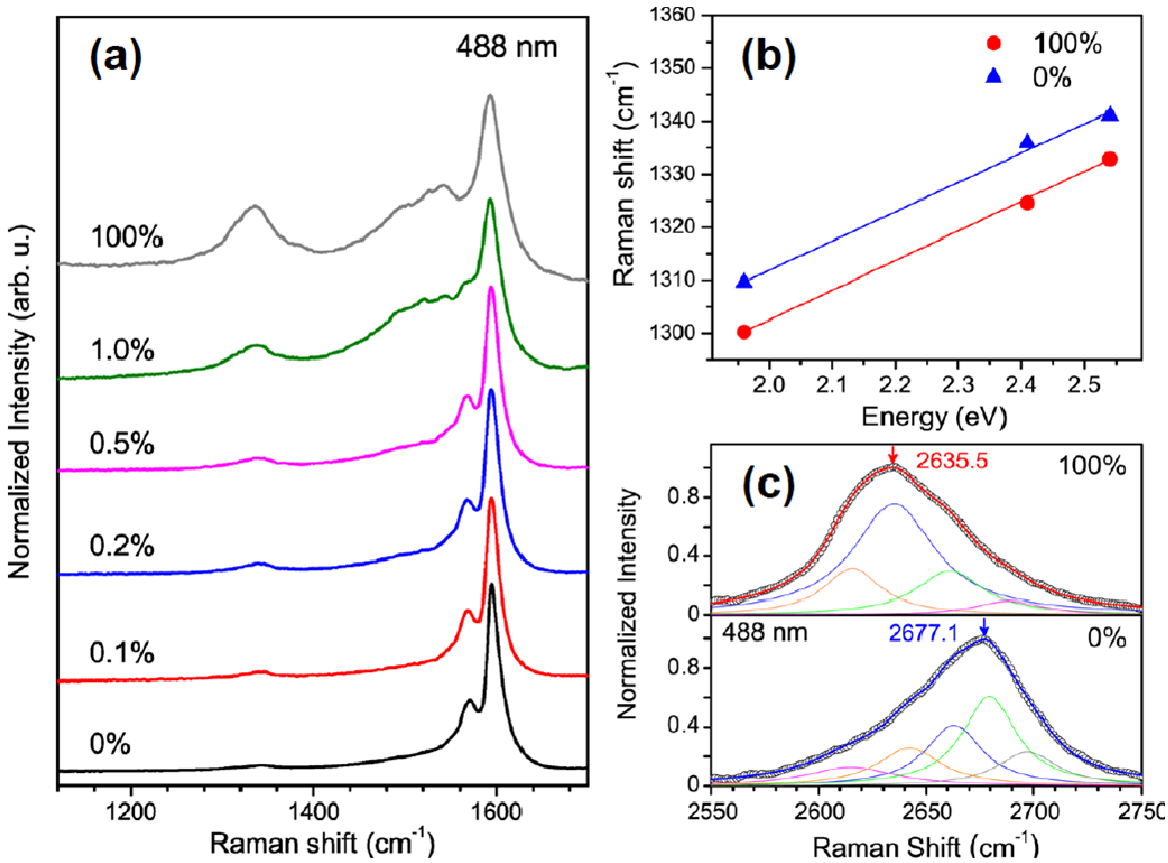

Fig. 5. (a) For 488 nm Raman excitation, the strong Fano lineshape clearly increases with a marginal increase in the concentration of acetonitrile in the feedstock. (b) The D band frequency is found to have an offset of 10 cm^{-1} for different E_{laser}, and (c) a large shift in the G′ line frequency is due to vastly different diameters (red and blue arrows represent G′ line positions for pure acetonitrile and pure ethanol, respectively).

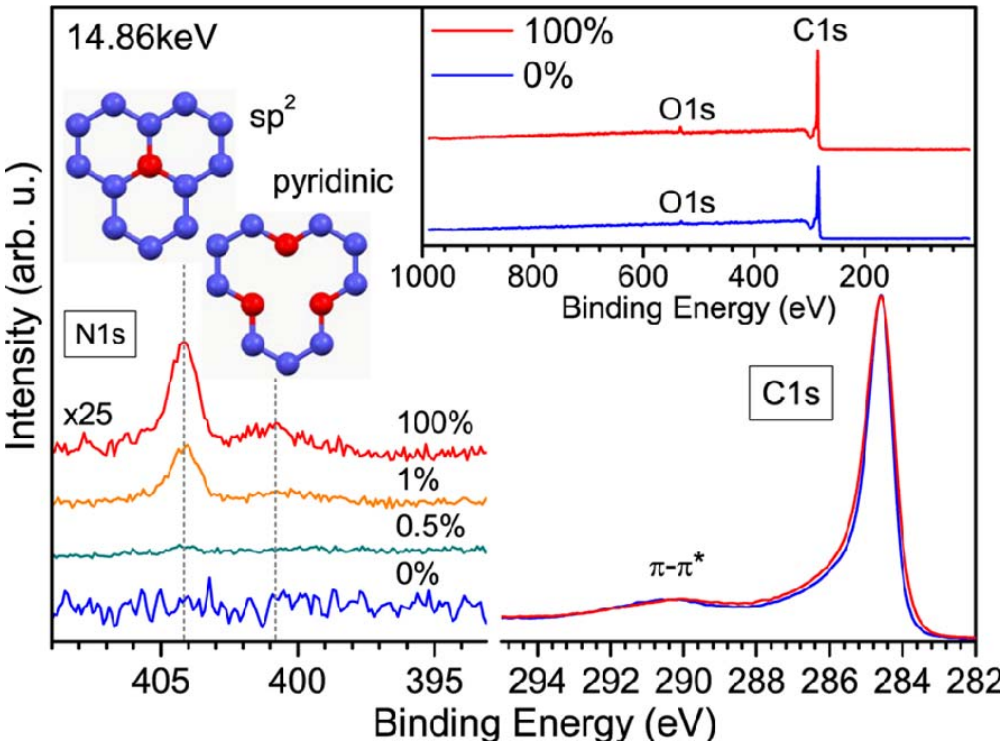

Fig. 6. The main panel shows C1s and N1s core level XPS spectra of vertically aligned SWCNT synthesized from different feedstocks. For synthesis from pure acetonitrile, the N1s profile is composed of ~1 at.% sp^2 and ~0.2 at.% pyridinic N (blue and red balls represent C and N atoms, respectively). Corresponding survey scans are provided in the inset.

these bounds. While the D line intensity is not specific to any certain kind of lattice distortion, N incorporation and pronounced curvature effects may well be expected in the small-diameter vertically aligned SWCNT.

Linear scaling of the D line position with laser energy (E_{laser}) and its diameter dependence have been reported earlier [34]. Figure 5b shows a plot of the D line frequencies against E_{laser}. The parallel dispersions for small-diameter pure acetonitrile-grown SWCNT and large-diameter pure ethanol-grown SWCNT are offset by 10 cm^{-1} with parallel slopes of 57 cm^{-1}/eV due to the diameter range differences. The structured G′ lines of both samples

were fitted using Lorentzian peaks. The G′ line for the pure ethanol sample was empirically fitted using five peaks at 2615, 2642, 2663, 2680, and 2697 cm^{-1}, whereas four peaks at 2616, 2635, 2661 and 2688 cm^{-1} were used for the pure acetonitrile sample. The offset in the G′ line frequency (peak maximum) at 488 nm (Fig. 5c) was found to be 41 cm^{-1} (from 2677–2636 cm^{-1}). These two distinct G′ positions have been observed as distinct components in undoped double-walled carbon nanotubes [35], dispersed HiPco SWCNT [36] and also N-doped SWCNT [37]. Reference [36] interprets the two different G′ positions as resonances of SWCNT with different diameters, whereas in Ref. [37] *n*-type doping from substitutional N was discussed as the origin of the lower frequency G′ peak. As discussed below, we also find a total of 1.2 at.% incorporated N in the pure acetonitrile-grown SWCNT based on XPS. Therefore, in our comparison of pure acetonitrile and ethanol samples intrinsic *n*-doping via sp^2 N *and* very different diameters with common resonances should be taken into account. By comparing to the G′ spectra in Refs. [35, 36] we conclude that the major effect is the common resonances from SWCNT with vastly different diameters. An additional influence of localized *n*-type doped N sites may be imposed on the discrete chirality pattern of the structured G′ peaks in pure acetonitrile and pure ethanol samples.

XPS spectra of SWCNT synthesized from mixed feedstock are shown in Fig. 6. The survey scans in the inset show a strong C1s peak and a weaker O1s peak. The sp^2 C1s peaks show an asymmetric Doniach-Sunjic lineshape. The well-established [15, 34, 38, 39] binding energy of the C1s at 284.6 eV is used for calibration. The chemical shifts of different bonding environments of incorporated N give rise to one narrow peak at 404.2 eV and a broadened peak at 400.8 eV. The narrow peak at 404.2 eV corresponds to substitutional sp^2 N, and the broad peak at 400.8 eV corresponds to different pyridinic N sites [40]. The atomic concentrations of 0.2 at.% pyridinic N and 1.0 at.% sp^2 N for SWCNT grown from pure acetonitrile were determined from the relative XPS peak intensities and the relative atomic

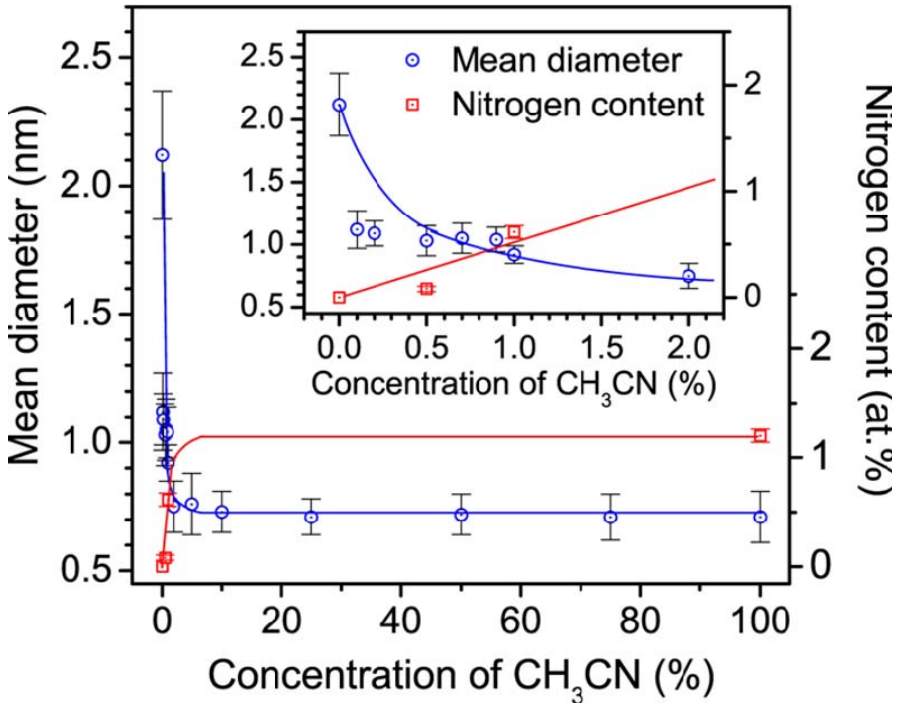

Fig. 7. A plot showing mean diameters of vertically aligned SWCNT based on UV-vis-NIR and XPS spectra of SWCNT synthesized using feedstock mixtures containing different concentration of acetonitrile in ethanol. A dramatic decrease in diameter is seen at low N content, followed by a saturation behavior for higher CH_3CN concentrations.

cross section of C:N=1:1.8 [41]. An approximate 1:1 ratio of sp^2 to pyridinic N is commonly reported for N-doped SWCNT [12-15], which is in contrast to the sp^2 dominance in sub-nm diameter vertically aligned SWCNT.

As revealed by the optical spectra discussed above, a marginal addition of acetonitrile (0.1%) causes the tube diameter to be dramatically reduced from 2.1 to 1.1 nm, whereas higher acetonitrile concentrations further reduce the mean diameter to 0.7 nm. XPS spectra indicate the N content is only gradually reduced when reducing the acetonitrile concentration from 5% to 1%, but a steep change in N content is observed between 0.5% and 1% acetonitrile. Since the N content at 5% and 1% is clearly beyond what a simple scaling by 5% or 1% would predict, we propose N in sp^2 carbon saturates slightly above 1 at.%. Very

remarkably, the saturated incorporation correlates with the reduction of the mean diameter (Fig. 7). The vividly displayed correlation in Fig. 7 points at the incorporation of N (mainly in sp^2 form) as the cause of diameter reduction.

It was recently proposed that even a few N atoms can affect the contact angle between Co catalyst particle and the graphitic walls due to stronger interaction of N to the catalyst [42]. Our results suggest that it may be plausible that a small amount of N incorporation may reform the catalyst and/or carbon structures near the catalyst site. The central consequence of this scenario would be that the equilibrium growth diameter should be independent of the initial nucleation diameter and therefore the catalyst morphology, and once N is incorporated into small-diameter SWCNT, the graphitic sp^2 N is also more likely to be formed than pyridinic N during the growth.

4. Conclusion

Combined observations from SEM, TEM, UV-vis-NIR, PLE, Raman and XPS clearly demonstrate that acetonitrile is indeed a viable carbon feedstock for the synthesis of vertically aligned SWCNT on flat substrates. Moreover, a compelling reduction in mean diameters from 2.1 nm for ethanol-grown SWCNT to just 0.7 nm for acetonitrile-grown vertically aligned SWCNT is reported. We establish a correlation between the reduction of the SWCNT diameter and an approximately one atomic percent saturated incorporation of nitrogen. This narrowing of nanotube diameter occurs for growth on flat substrates as well as on zeolite powder, indicating that N takes an active role in yielding sub-nm diameter SWCNT, independent of catalyst preparation. Catalyst-particle-independent diameter control by trace amounts of heteroatoms represents a versatile pathway for the direct synthesis of engineered SWCNT.

Acknowledgements

Part of this work was financially supported by Grants-in-Aid for Scientific Research (19051016, 19054003 and 22226006), and the Global COE Program "Global Center for Excellence for Mechanical Systems Innovation". TT acknowledges support from the Office of Higher Education Commission, Thailand. CK acknowledges the Austrian Academy of Sciences for the APART fellowship A-11456.

References

[1] Bachilo SM, Balzano L, Herrera JE, Pompeo F, Resasco DE, Weisman RB. Narrow (n,m)-distribution of single-walled carbon nanotubes grown using a solid supported catalyst. J Am Chem Soc 2003; 125(37):11186-7.

[2] Miyauchi Y, Chiashi S, Murakami Y, Hayashida Y, Maruyama S. Fluorescence spectroscopy of single-walled carbon nanotubes synthesized from alcohol. Chem Phys Lett 2004; 387(1-3):198-203.

[3] Kitiyanan B, Alvarez WE, Harwell JH, Resasco DE. Controlled production of single-wall carbon nanotubes by catalytic decomposition of CO on bimetallic Co-Mo catalysts. Chem Phys Lett 2000; 317(3-5):497-503.

[4] Wang B, Yang Y, Li LJ, Chen Y. Effect of different catalyst supports on the (n,m) selective growth of single-walled carbon nanotube from Co-Mo catalyst. J Mater Sci 2009; 44(12):3285-95.

[5] Li XL, Tu XM, Zaric S, Welsher K, Seo WS, Zhao W, et al. Selective synthesis combined with chemical separation of single-walled carbon nanotubes for chirality selection. J Am Chem Soc 2007; 129(51):15770-1.

[6] Wang H, Wang B, Quek XY, Wei L, Zhao JW, Li LJ, et al. Selective synthesis of (9,8) single walled carbon nanotubes on cobalt incorporated TUD-1 catalysts. J Am Chem Soc 2010; 132(47):16747-9.

[7] Suzuki S, Asai N, Kataura H, Achiba Y. Formation of single-wall carbon nanotubes in Ar and nitrogen gas atmosphere by using laser furnace technique. Eur Phys J D 2007; 43(1-3):143-6.

[8] Cassell AM, Raymakers JA, Kong J, Dai HJ. Large scale CVD synthesis of single-walled carbon nanotubes. J Phys Chem B 1999; 103(31):6484-92.

[9] Xiang R, Einarsson E, Okawa J, Miyauchi Y, Maruyama S. Acetylene-accelerated alcohol catalytic chemical vapor deposition growth of vertically aligned single-walled carbon nanotubes. J Phys Chem C 2009; 113(18):7511-5.

[10] Hafner JH, Bronikowski MJ, Azamian BR, Nikolaev P, Rinzler AG, Colbert DT, et al. Catalytic growth of single-wall carbon nanotubes from metal particles. Chem Phys Lett 1998; 296(1-2):195-202.

[11] Cheng HM, Li F, Su G, Pan HY, He LL, Sun X, et al. Large-scale and low-cost synthesis of single-walled carbon nanotubes by the catalytic pyrolysis of hydrocarbons. Appl Phys Lett 1998; 72(25):3282-4.

[12] Ayala P, Arenal R, Loiseau A, Rubio A, Pichler T. The physical and chemical properties of heteronanotubes. Rev Mod Phys 2010; 82(2):1843-85.

[13] Ayala P, Grüneis A, Kramberger C, Rümmeli MH, Solorzano IG, Freire FL, Jr., et al. Effects of the reaction atmosphere composition on the synthesis of single and multiwalled nitrogen-doped nanotubes. J Chem Phys 2007; 127(18):184709-14.

[14] Ayala P, Grüneis A, Gemming T, Büchner B, Rümmeli MH, Grimm D, et al. Influence of the catalyst hydrogen pretreatment on the growth of vertically aligned nitrogen-doped carbon nanotubes. Chem Mater 2007; 19(25):6131-7.

[15] Ibrahim EMM, Khavrus VO, Leonhardt A, Hampel S, Oswald S, Rümmeli MH, et al. Synthesis, characterization, and electrical properties of nitrogen-doped single-walled carbon nanotubes with different nitrogen content. Diam Relat Mater 2010; 19(10):1199-206.

[16] Pint CL, Sun ZZ, Moghazy S, Xu YQ, Tour JM, Hauge RH. Supergrowth of nitrogen-doped single-walled carbon nanotube arrays: active species, dopant characterization, and doped/undoped heterojunctions. ACS Nano 2011; 5(9):6925-34.

[17] Ayala P, Arenal R, Rümmeli M, Rubio A, Pichler T. The doping of carbon nanotubes with nitrogen and their potential applications. Carbon 2010; 48(3):575-86.

[18] Bulusheva LG, Okotrub A, Kudashov AG, Shubin YV, Shlyakhova E, Yudanov NF, et al. Effect of Fe/Ni catalyst composition on nitrogen doping and field emission properties of carbon nanotubes. Carbon 2008; 46(6):864-9.

[19] Xia YD, Mokaya R, Grant DM, Walker GS. A simplified synthesis of N-doped zeolite-templated carbons, the control of the level of zeolite-like ordering and its effect on hydrogen storage properties. Carbon 2011; 49(3):844-53.

[20] Cui TX, Lv RT, Huang ZH, Zhu HW, Zhang J, Li Z, et al. Synthesis of nitrogen-doped carbon thin films and their applications in solar cells. Carbon 2011; 49(15):5022-8.

[21] Murakami Y, Chiashi S, Miyauchi Y, Hu MH, Ogura M, Okubo T, et al. Growth of vertically aligned single-walled carbon nanotube films on quartz substrates and their optical anisotropy. Chem Phys Lett 2004; 385(3-4):298-303.

[22] Xiang R, Zhang ZY, Ogura K, Okawa J, Einarsson E, Miyauchi Y, et al. Vertically aligned (13)C single-walled carbon nanotubes synthesized by no-flow alcohol chemical vapor deposition and their root growth mechanism. Jpn J Appl Phys 2008; 47(4):1971-4.

[23] Murakami Y, Miyauchi Y, Chiashi S, Maruyama S. Direct synthesis of high-quality single-walled carbon nanotubes on silicon and quartz substrates. Chem Phys Lett 2003; 377(1-2):49-54.

[24] Murakami Y, Maruyama S. Detachment of vertically aligned single-walled carbon nanotube films from substrates and their re-attachment to arbitrary surfaces. Chem Phys Lett 2006; 422(4-6):575-80.

[25] Murakami Y, Miyauchi Y, Chiashi S, Maruyama S. Characterization of single-walled carbon nanotubes catalytically synthesized from alcohol. Chem Phys Lett 2003; 374(1-2):53-8.

[26] Maruyama S, Kojima R, Miyauchi Y, Chiashi S, Kohno M. Low-temperature synthesis of high-purity single-walled carbon nanotubes from alcohol. Chem Phys Lett 2002; 360(3-4):229-34.

[27] Wu ZC, Chen ZH, Du X, Logan JM, Sippel J, Nikolou M, et al. Transparent, conductive carbon nanotube films. Science 2004; 305(5688):1273-6.

[28] Araujo PT, Doorn SK, Kilina S, Tretiak S, Einarsson E, Maruyama S, et al. Third and fourth optical transitions in semiconducting carbon nanotubes. Phys Rev Lett 2007; 98(6):067401-4.

[29] Fantini C, Jorio A, Souza M, Strano MS, Dresselhaus MS, Pimenta MA. Optical transition energies for carbon nanotubes from resonant Raman spectroscopy: environment and temperature effects. Phys Rev Lett 2004; 93(14):147406-4.

[30] Piscanec S, Lazzeri M, Robertson J, Ferrari AC, Mauri F. Optical phonons in carbon nanotubes: Kohn anomalies, Peierls distortions, and dynamic effects. Phys Rev B 2007; 75(3):035427-22.

[31] Dresselhaus MS, Dresselhaus G, Saito R, Jorio A. Raman spectroscopy of carbon nanotubes. Phys Rep 2005; 409(2):47-99.

[32] Dubay O, Kresse G, Kuzmany H. Phonon softening in metallic nanotubes by a Peierls-like mechanism. Phys Rev Lett 2002; 88(23):235506-9.

[33] Kataura H, Kumazawa Y, Maniwa Y, Umezu I, Suzuki S, Ohtsuka Y, et al. Optical properties of single-wall carbon nanotubes. Synthetic Met 1999; 103(1-3):2555-8.

[34] Brown SDM, Jorio A, Dresselhaus MS, Dresselhaus G. Observations of the D-band feature in the Raman spectra of carbon nanotubes. Phys Rev B 2001; 64(7):073403-6.

[35] Pfeiffer R, Kuzmany H, Simon F, Bokova SN, Obraztsova E. Resonance Raman scattering from phonon overtones in double-wall carbon nanotubes. Phys Rev B 2005; 71(15):155409-16.

[36] Cardenas JF, Gromov A. Double resonance Raman scattering in solubilised single walled carbon nanotubes. Chem Phys Lett 2007; 442(4-6):409-12.

[37] Maciel IO, Anderson N, Pimenta MA, Hartschuh A, Qian HH, Terrones M, et al. Electron and phonon renormalization near charged defects in carbon nanotubes. Nat Mater 2008; 7(11):878-83.

[38] Ayala P, Grüneis A, Gemming T, Grimm D, Kramberger C, Rümmeli MH, et al. Tailoring N-doped single and double wall carbon nanotubes from a nondiluted carbon/nitrogen feedstock. J Phys Chem C 2007; 111(7):2879-84.

[39] Lim SH, Elim HI, Gao XY, Wee ATS, Ji W, Lee JY, et al. Electronic and optical properties of nitrogen-doped multiwalled carbon nanotubes. Phys Rev B 2006; 73(4):045402-7.

[40] Usachov D, Vilkov O, Grüneis A, Haberer D, Fedorov A, Adamchuk VK, et al. Nitrogen-doped graphene: efficient growth, structure, and electronic properties. Nano Lett 2011; 11(12):5401-7.

[41] Scofield JH. Hartree-Slater subshell photoionization cross-sections at 1254 and 1487 eV. J Electron Spectrosc 1976; 8(2):129-37.

[42] O'Byrne JP, Li Z, Jones SLT, Fleming PG, Larsson JA, Morris MA, et al. Nitrogen-doped carbon nanotubes: growth, mechanism and structure. Chemphyschem 2011; 12(16):2995-3001.